Journal of Zhejiang University-SCIENCE A (Applied Physics & Engineering)
ISSN 1673-565X (Print); ISSN 1862-1775 (Online)
www.jzus.zju.edu.cn; www.springerlink.com
E-mail: jzus@zju.edu.cn

Assessment of integration method for displacement determination using field accelerometer and geophone data*

F. LAMAS-LOPEZ†[1,2], Y. J. CUI[1], S. COSTA D'AGUIAR[3], N. CALON[2]

([1]*Ecole des Ponts ParisTech, Laboratoire Navier/CERMES, Marne-la-Vallée, France*)

([2]*SNCF, Direction Projet, Systèmes & Ingénierie, Département Ligne, Voie et Environnement, La Plaine Saint-Denis, France*)

([3]*SNCF, Direction Innovation & Recherche, Paris, France*)

†E-mail: lamas1987@gmail.com

Received Mar. 6, 2016; Revision accepted Dec. 16, 2016; Crosschecked June 16, 2017

Abstract: A conventional French railway track was instrumented with accelerometers and geophones at three depths: sleeper (surface), interlayer (ITL, z=−0.93 m), and transition layer (TL, z=−1.20 m). A linear variable differential transformer (LVDT) was also used to monitor the displacement at the sleeper level. The recorded data allow the integration method (double for accelerometer and simple for geophone) for displacement determination to be assessed. Several questions need to be addressed prior to the selection of an adequate monitoring system: definition of signal filtering processes, influence on results of the different loading wavelengths, repeatability of measurements, train speed and axle load impact and their ranges of validity for each sensor. It was found that the main frequencies that caused more than 95% of the displacement of the monitored materials are in the low frequency range: <25 Hz for trains running up to 200 km/h. For an intercity train, the low frequencies are normally excited by long wavelengths, for instance, those corresponding to the 1/2 coach distance (λ=13.20 m), the bogies distance (λ=6.3 m), and the axle distance (λ=2.8 m). Comparison between the displacements deduced from the records of accelerometer and geophone and obtained from the records of LVDT shows quite consistent results; the mean displacement amplitudes obtained from accelerometers differ by only 20% from the LVDT records. The train speed does not have a strong effect on the obtained differences between sensors. The embedded sensors also gave consistent displacement results for each analysed depth. Moreover, the displacement amplitudes caused by different axle loads (locomotive or passenger coach) are distinguishable for all sensors at all depths. This validates the integration method used for the displacement determination.

Key words: Railway track; Vibrations; Accelerometer; Geophone; Linear variable differential transformer (LVDT); Integration method; Deflection amplitude estimation; Measurement repeatability

http://dx.doi.org/10.1631/jzus.A1600212 **CLC number:** U28

1 Introduction

Vibration monitoring has become one of the main methods to analyse the mechanical behaviour of infrastructure. In the railway field, monitoring track element displacements can bring valuable information about infrastructure use conditions and its state (Galvín and Domínguez, 2007). Field monitoring of conventional railway sites using different vibration and displacement sensors was performed by several studies. Madshus and Kaynia (2000) used particle image velocimetry to evaluate sleeper vertical deflection and analyse the train speed impact at the Ledsgard site in Sweden. Hall *et al*. (2003) also investigated the Ledsgard site, measuring vertical deflections with extensometers installed at different depths. Similar results were obtained using the multi-depth deflectometers (MDD) system (Fröhling,

* Project supported by the Influence de la Vitesse sur le Comportement de la Structure de Assise (INVICSA) Research Project Funded by SNCF-RESEAU and the Association Nationale de Recherche et Technologie (ANRT) with a Convention Industrielle pour la Formation dans la Recherché (CIFRE) (No. 2012/1150)

ORCID: F. LAMAS-LOPEZ, http://orcid.org/0000-0002-9434-1484

1997; Hendry *et al.*, 2013; Mishra *et al.*, 2014) allowing the evaluation of the deflections of the different layers of a platform. Other measurements as accelerations using piezo-electric and capacitive accelerometers or particles velocities using geophones were also performed on track elements such as sleepers (Galvín and Domínguez, 2009; Le Pen *et al.*, 2014), or in track-bed materials (Cui *et al.*, 2014). It was found that signal processing has a strong influence on results when accelerometer or geophone signals are integrated. Moreover, the model and type of sensors have to be adapted to railway loadings (frequencies and amplitudes) to obtain accurate measurements.

Train loadings develop a dynamic excitation on track materials. Even if linear variable differential transformer (LVDT) or MDD devices are able to measure deflections under loading (regarding exclusively very low frequencies), track materials response during train dynamic excitation should be assessed using devices allowing to measure a wider range of frequencies as accelerometers or geophones (Connolly *et al.*, 2013). However, a direct measurement of the deflection is necessary to perform a first comparison with the results obtained by other indirect methods as accelerometers or geophones. The excited frequencies on the sensor depend on train speed and the wavelengths of loading, which also depend on the geometrical characteristics of the train. The amount of energy (in frequency domain) transmitted by the train through different track materials could be assessed by analysing the power spectrum density (PSD) during loading (Kouroussis *et al.*, 2014). In the PSD the impact of every wavelength present in the train/track system on the track response can be assessed. Regarding the effect of sensor position on the track, the train excitation effects (deflection amplitude or PPV) on track materials behaviour exponentially attenuate in distance from loading source (Connolly *et al.*, 2015; Kouroussis *et al.*, 2015). Consequently, only the measurements performed by different devices at equivalent positions on the track should be compared.

Bowness *et al*. (2007) studied the accuracy of the integration method comparing geophone and particle image velocimetry measurements (PIV) in terms of peak-to-peak displacement amplitudes. They developed a filtering method for geophone signals, eliminating very low cut-off frequencies with a high-pass filter (f_c=0.20 Hz) and filtering the noise in the laboratory from the signal with a low-pass filter (f_c=1 Hz). Their measurements were performed in the laboratory and at four different sites. This integration method was applicable for train speed ranging from 25 km/h to 100 km/h within the geometrical characteristics of the rolling stock. Le Pen *et al.* (2014) amplified the passband of filters for geophone signals from 1 Hz to 30 Hz (natural frequency of geophones: 1 Hz), but some problems remained in the shape of the signal at the beginning and the end of the signal section containing train loading, mainly caused by high-pass filters, very close to the natural frequency of the sensors. Costa *et al.* (2012) considered low-pass filters at higher frequencies (f_c=60 Hz) to eliminate noise and amplitudes caused by small wavelengths. When low-pass filters are applied on signals to avoid noise, one of the main assumptions made is that the signal excitation (train loading) is short (when train speed is high). It is reasonable to admit in that case that the background noise does not change significantly during the excitation, and thus the noise might be considered as stationary (Kyoya and Arakawa, 2009; Zuada-Coelho, 2011) even if noise and signal are not statistically independent variables (Thong *et al.*, 2002; Stiros, 2008). The covariance between noise and signal for modern sensors is close to zero. The high-pass filter, applied after each integration by some authors, is used to correct the low frequency error induced by the integration (Trifunac, 1971; Boore and Bommer, 2005). The integration method presented by Bowness *et al.* (2007) constitutes the basis of other methods as the spectral substraction method developed by Zuada-Coelho (2011). This method separates noise from signal by filtering very low frequencies (f_c=0.20 Hz) prior to integrating and reconstituting the signal. Most of the authors who studied strong-motion recordings due to earthquakes concluded that the estimation of permanent displacements is complicated because of the difficulties in computing the low frequency response of the displacement (Boore, 2001; Graizer, 2010). In addition to low- and high-pass filters, baseline corrections are presented for adjustments in the low-frequency range (Yang *et al.*, 2006). For trains running up to 300 km/h, the most energetic frequencies

excited by displacement signals are low-frequencies (first 5 Hz) compared to the frequency excitation of geophones (first 10 Hz) and accelerometers (first 30 Hz) (Degrande and Schillemans, 2001; Galvín and Domínguez, 2009; Costa *et al.*, 2012). These excitation frequencies are taken into account when the specifications of sensors are defined, to adapt the installed sensor to the train loadings. Low frequencies are the reason of most of displacement amplitudes in a signal; moreover, low frequencies damp less quickly in distance compared to high frequencies (Connolly *et al.*, 2014). Signals from capacitive accelerometers are more appropriate to be integrated because low-frequencies are better recorded compared to piezo-electric accelerometers. This explains why capacitive accelerometers are widely used in track-bed where acceleration amplitudes are lower (Ferreira and López-Pita, 2015). The effect of frequency loading in depth was studied by Priest *et al.* (2010), showing a decrease of energy from the surface to track-bed materials, and a subsequent displacement decrease from track-surface to deeper positions. Vertical displacements were studied using video on surface and with geophones mounted on a carrier in four boreholes created at four different depths (Priest *et al.*, 2010). Integration method was applied based on the previous studies of the same group (Bowness *et al.*, 2007). Priest and Powrie (2009) also applied the integration method to evaluate the elastic parameters of a track, such as the elastic modulus, from sleeper deflection amplitudes under train loading. The results showed a decrease of elastic modulus with the increase of train speed.

Even though numbers of studies were conducted around the integration method, there are still some open questions to be assessed. This paper aims at addressing the following questions: the influence of each wavelength loading (bogies distance, axle distance, coach distance, etc.) on the displacement estimations, the range of validity and repeatability of the integration method results, and the train speed and axle load impact on the deflections. The values of displacement are obtained from accelerometers, geophones, and LVDT, using data from an instrumented conventional track. The answers to the questions could help better understand the integration method and the factors that may influence the process.

2 Methods

The monitored site is located in Vierzon (Center Region of France). The track is representative of the conventional French railway network. The site is composed of two parallel tracks in an alignment. Consequently, the load arriving to both rails of a track is supposed to be the same. The cross section of the experimental site (Fig. 1) consists of 50 cm fresh ballast, 40 cm ITL (interlayer soil), 20 cm TL (transition layer soil), the subgrade being at z=−1.20 m depth from the running surface of rails (Lamas-Lopez *et al.*, 2016a; 2016b).

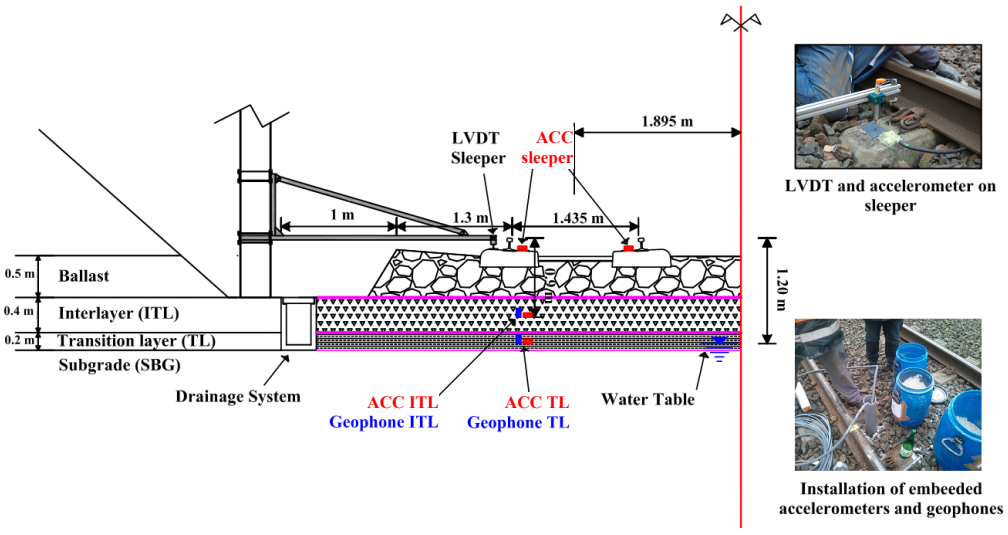

Fig. 1 Cross section of the monitored zone and sensors' positions in the track

In this study, piezo-electric accelerometers and LVDT sensors were installed on sleeper (surface); capacitive accelerometers and geophones were installed in two different depths below the track: one in the interlayer (ITL, z=−0.93 m) and two in the transition layer (TL, z=−1.20 m). The installed geophones are able to measure a frequency ranging from 0.3 Hz to 8000 Hz, and their working range is ±15 m/s. The same geophone model used by Bowness *et al*. (2007) was selected, but with lower natural frequency (f=0.3 Hz), in order to have better measurements in low frequency range and to enlarge the range of validity related to train speed depending on the applied high-pass filters cut-off frequencies. The sensors' positions are shown in Fig. 1 and more specifications are described in Table 1.

The LVDT sensor was installed at an aluminium structure anchored to a catenary post (Fig. 1) to measure sleeper surface deflection. Note that this kind of sensor is able to measure the deflection of a point directly. Several studies measured on-surface deflections directly using a motion-cam that records a target at rail while trains ran on the site (Madshus and Kaynia, 2000; Hall, 2003; Bowness *et al.*, 2007; Hendry *et al.*, 2010; Costa *et al.*, 2012).

A typical response of the three different sensors during the passage of a train is shown in Fig. 2. The signals correspond to the passage of an intercity train running at 200 km/h, the maximal service speed of the monitored line. The signals' first part, at the left, corresponds to the applied load by four axles of a BB22000 or BB26000 series locomotive (Q= 225 kN/axle), followed by seven 'Corail' passenger coaches resulting in 28 axles (Q=105 kN/axle).

The scheme of the integration method is presented in Fig. 3. To obtain displacements, raw accelerometers signals are filtered and integrated twice, while geophone signals are filtered and integrated once only.

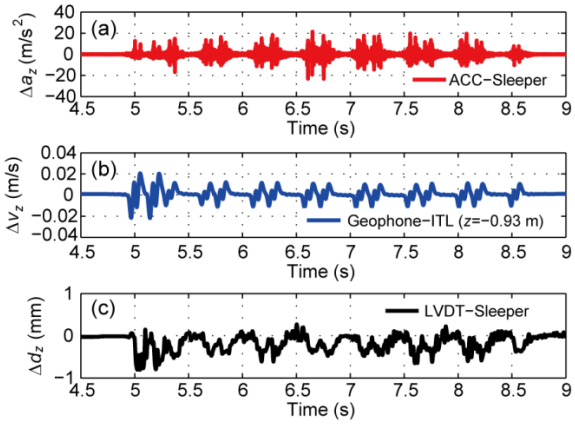

Fig. 2 Raw vertical acceleration signal on sleeper (a), raw vertical geophone signal (−0.93 m in the track) (b), and LVDT displacement signal on sleeper during the intercity train passage at v_I=200 km/h (c)

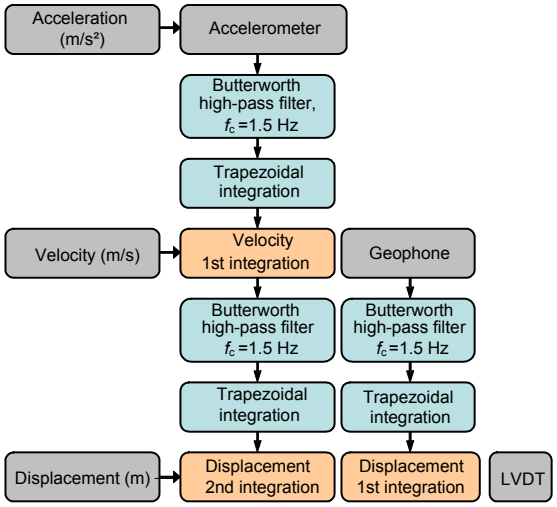

Fig. 3 Scheme of the integration procedure of the signals from accelerometers and geophones to estimate displacements

Table 1 Installed sensors specifications

Sensor	Model	Capacity	Dimensions	Other specifications
On-sleeper accelerometers	ICP PCB-601D01	±500 m/s²	22 mm×22 mm ×49.3 mm	Spectral noise at 10 Hz: 31.0 (μm/s²)·Hz$^{-1/2}$; frequency range: 0.47–10 000 Hz
Embedded accelerometers	TML ARH-10 A	±10 m/s²	16 mm×16 mm ×28 mm	Rated output approx.: 0.5 mV/V (1000×10^{-6} strain); frequency response: 0.5–50 Hz; natural frequency: 100 Hz
Geophones	ION LF-24/0.3 Hz	±15 m/s	ø: 32.5 mm; L: 78.6 mm	Operational temperature: −20–60 °C; lower frequency: 0.3 Hz; protection index: IP65
LVDT	OMEGA LD661-10	10 mm	ø: 19 mm; L: 169 mm	Operational temperature: 0–65 °C; vibration (sinudoidal): 10–50 Hz, 1–10 g·rms linear; protection index: IP68

One high-pass filter is needed prior to each integration, in order to avoid the baseline effect on the integration result (Boore, 2001; 2003; Boore *et al.*, 2002; Boore and Bommer, 2005; Yang *et al.*, 2006). Then, a low cut-off frequency of f_c=1.5 Hz is applied, allowing eliminating the very low frequencies that are not measured with accuracy by accelerometers and geophones. If these frequencies, lower than 1 Hz, were integrated, the baseline effect would appear due to the sensors themselves. This high-pass cut-off frequency was chosen for two reasons. The first one is that almost all the intercity trains involved on the site ran faster than v_T=80 km/h, the half coach wavelength being the lowest frequency of the four most energetic peaks caused by train loadings (Fig. 4). To obtain a valid displacement amplitude this frequency may not be filtered for this train speed (f=1.68 Hz). The second reason was that for cut-off frequencies lower than f_c=1.5 Hz (using a high-pass Butterworth filter of the fifth order, Fig. 5), the integrated signals from accelerometers presented a baseline defect and displacement signal shapes are no longer consistent with the axles and bogies loadings. This was due to the accelerometer frequency measurement range specifications. All the signal amplitudes originated from frequencies lower than f=1 Hz (close to the natural frequency of sensors) might be totally filtered (filter magnitude close to 0 at 1 Hz) in order to avoid baseline defects after integration (Fig. 5).

A Butterworth filter was used in this study, because it was easier to be defined compared to the elliptical or Chebyshev one. Only two parameters are needed to define a Butterworth filter: cut-off frequency and filter order. By contrast, five parameters are needed with the elliptical filter. Moreover, unlike the elliptical filter that eliminates some amplitude variations, the Butterworth filter takes exactly 100% of the amplitude of the original signal after the cut-off frequency (Cui *et al.*, 2014). The Butterworth filter also allows a gradual transition of the amplitude of the signal at frequencies around the cut-off frequency (for high-pass filter, Fig. 5) without modifying the signal amplitudes. On the contrary, the elliptical filter sharply eliminates the signal at the cut-off frequency. The order in Butterworth filter determines the filter 'slope' after the cut-off frequency. The higher the order, the higher the filter 'slope' at the cut-off frequency. The filters used in this study have an order 5, which is high enough to avoid very low frequencies (lower than 1 Hz) with a cut-off frequency of f_c=1.5 Hz.

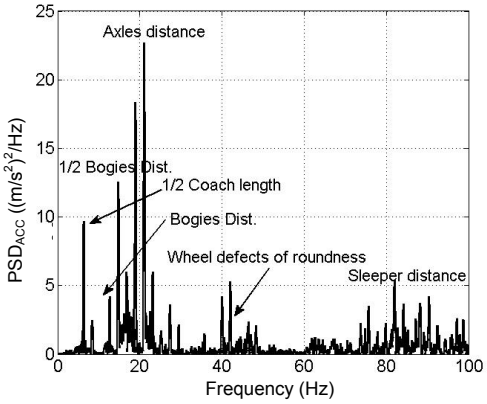

Fig. 4 Analysis of power spectrum density (PSD) of an accelerometer at the sleeper after a passage of an intercity train running at v_T=200 km/h

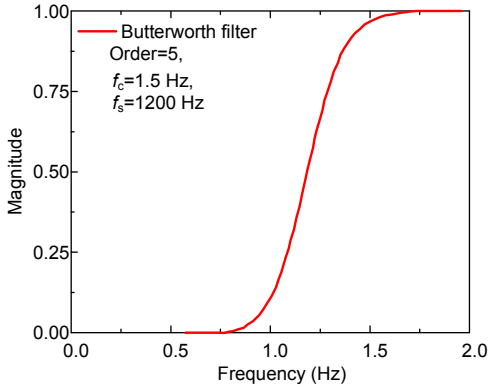

Fig. 5 High-pass Butterworth filter of the fifth order (f_c=1.5 Hz and the sampling frequency f_s=1200 Hz)

Once the filter parameters were obtained, the filter was applied in both directions from the beginning to the end of the signal and backwards to remove the phase distortion (Kornylo and Jain, 1974). After filtering, a trapezoidal integration was performed. The boundary conditions for the signal integrations were velocity and displacement that were set to zero at the beginning and the end of the signal. The integration of a discrete signal, like the accelerometer one, can be addressed by considering a trapezoidal rule as shown in Eqs. (1) and (2) (Zuada-Coelho, 2011).

$$v(n)=v(n-1)+\frac{\Delta t}{2}\left[a(n)+a(n-1)\right], \qquad (1)$$

$$d(n)=d(n-1)+\frac{\Delta t}{2}\left[v(n)+v(n-1)\right], \qquad (2)$$

where $v(n)$ and $d(n)$ are the first integration (velocity) and second integration (displacement) of the discrete acceleration signal $a(n)$, respectively.

3 Results and discussion

As mentioned above, to avoid the baseline effect, a high-pass filter is needed to eliminate very low frequencies before integrate the signals. However, low-pass filters could be also applied before each integration step in order to eliminate the amplitudes originated from high frequencies. This implies that it is possible to analyse the influence of each excited frequency on the total displacement. Following the method presented in Section 2, an additional low-pass Butterworth filter of order 5 was applied to the signal before being integrated, changing the cut-off frequencies from 1.5 Hz to 100 Hz. Thereby, it is possible to estimate certain amplitudes from the total displacement signal. Note that each frequency excitation f corresponds to a wavelength λ of the railway system at a given train speed v (Auersch, 1994; Müller-Boruttau and Breitsamer, 2004), i.e.,

$$f=\frac{v}{\lambda}. \qquad (3)$$

For instance, if the axles-distance in a locomotive is λ=2.8 m, and the locomotive is running at v=200 km/h, the excited frequency f=19.8 Hz.

The accelerometer, geophone, and LVDT signals were recorded during the passage of an intercity train as described in Section 2 (locomotive+7 coaches), running at 200 km/h. The locomotive has four axles on two bogies and each coach has four axles, too. For acceleration and particle velocity, each 'axle peak' is considered as the maximum positive value around each axle loading for each train. However, in the displacement signals, the amplitudes are calculated as shown in Fig. 6, from axle peak to middle-coach peak (Bowness *et al.*, 2007; Le Pen *et al.*, 2014), giving the sleeper rest position for each axle load in the train (locomotive and coaches). The amplitude accounted for in the following figures is the average of each typology of axles for each train (average of four axles for locomotive, and average for four times the number of coach axles for the coaches). The shape of the signal before and after the train passage is due to the border conditions in each integration process.

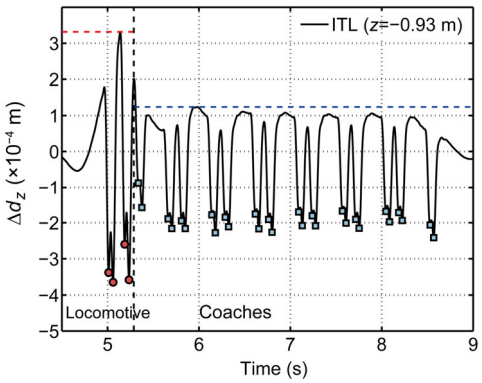

Fig. 6 Peak-to-peak displacement estimation obtained from a doubled-integrated accelerometer signal installed in interlayer (z=−0.93 m). Signal corresponds to an intercity train running at 200 km/h. Different axle loads are considered

Fig. 7a presents the displacement amplitudes under the train load by locomotive and coach, obtained at each cut-off frequency with a low-pass filter, every 0.5 Hz from 1.5 to 100 Hz, for two accelerometers installed on a sleeper. This allows the assessment of the repeatability of the performed measurements in similar positions and with similar sensors. The two accelerometers are installed at both sides of the same sleeper. Fig. 7b is a zoom of the first 25 Hz where most displacement amplitudes are developed. Three frequency lines corresponding to the main wavelength excitations are also presented in the figure: the 1/2 coach distance (λ=13.2 m), the bogies distance (λ=6.3 m), and the axles distance (λ=2.8 m). It appears that the estimated displacement amplitudes for both accelerometers are similar for all the considered frequencies, suggesting that the results at equivalent positions can be compared. For different axle loads (locomotive and coach), it is possible to identify different displacement amplitudes. It appears that more than 95% of the total displacement is caused by the first 25 Hz of excitation, i.e., by wavelengths longer than the axle-distance. Beyond 25 Hz, the displacement amplitude tends to stabilise.

Train loadings from wavelengths smaller than axle-distance (λ=3 m), that cause loading frequencies in the range from 25 to 100 Hz, did not increase the displacement amplitudes by more than 5% even though some energy was transmitted by different elements of the railway system (as sleepers or rail defects) in this frequency range (Fig. 4).

Figs. 8a and 8b present the displacement amplitude estimated from signals of embedded accelerometers and geophones versus cut-off frequencies

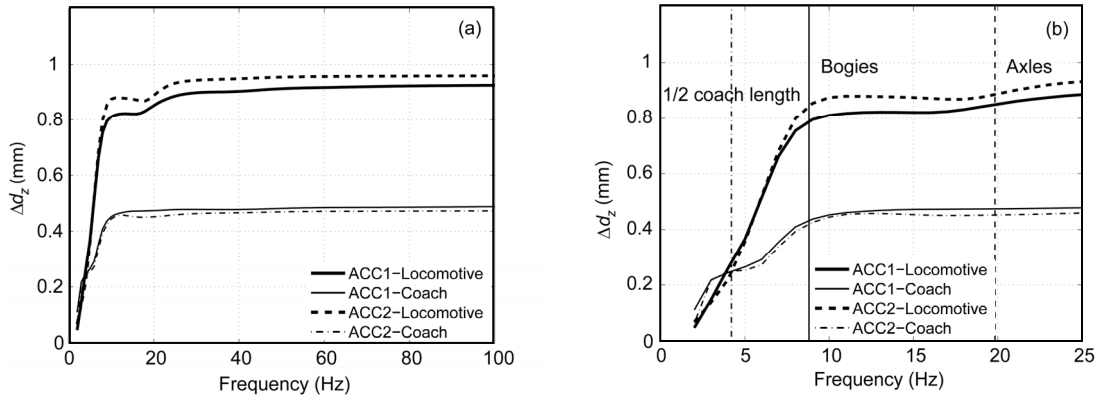

Fig. 7 (a) Comparison of the displacement amplitudes variation with frequency estimated after double integrating the signals of the accelerometer installed on the left side (ACC1) and right side (ACC2) of the same sleeper. The considered loading was by an intercity train running at 200 km/h. (b) A zoom of the first 25 Hz response. Three frequencies corresponding to the elements from the railway loading are represented

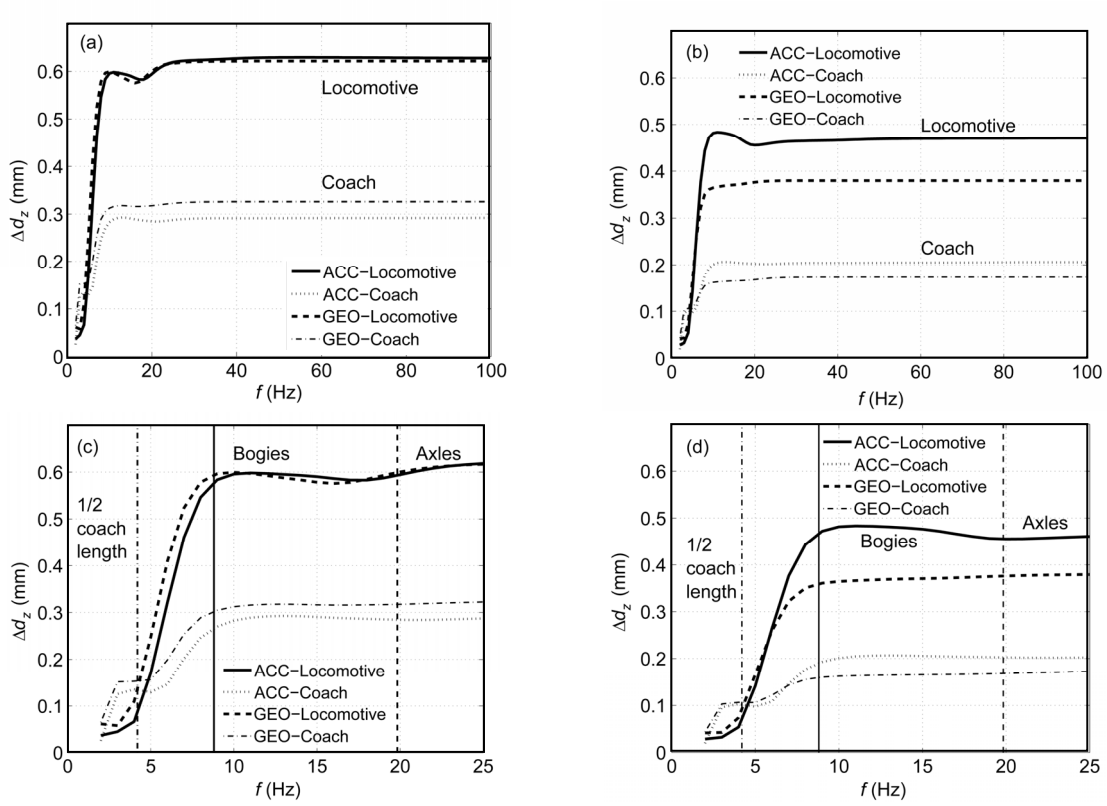

Fig. 8 Comparison between the displacement amplitudes estimated from the signals of geophones (first integration) and the displacement amplitudes estimated after double integrating the accelerometer signals for an intercity train running at 200 km/h. Two depths are considered: (a) interlayer (ITL, z=−0.93 m) and (b) transition layer (TL, z=−1.20 m). The corresponding zooms for the first 25 Hz are presented in (c) and (d), respectively

(low-pass filter changes while high-pass filter is always the same), in embedded positions: ITL and TL, respectively. The corresponding zooms for the first 25 Hz are presented in Figs. 8c and 8d, respectively. As in Fig. 7b, three frequency lines corresponding to the main wavelength excitations are indicated to make easier the analysis of the total displacement amount provided by each frequency. Similar displacement amplitudes are obtained from geophone and accelerometer estimations after integrations (for locomotive and coaches). In the ITL, there is a difference smaller than 0.02 mm of the total displacement amplitude (6.5% of displacement amplitude). For the TL, there is a 0.09 mm difference (18% of displacement amplitude) for the locomotive, and a difference of 0.02 mm (10% of displacement amplitude) for the coach. In addition, their amplitude contributions are similar for both sensors. As seen from Fig. 7, for the embedded sensors, more than 95% of the total displacement amplitude is caused by the first 25 Hz excitation for intercity trains running at v_T=200 km/h. Table 2 shows the percentage of the total displacement amplitude obtained at each of the four frequencies highlighted. Note that the total displacement amplitude is considered as the amplitude obtained in the case without application of low-pass filter to the signal. For the intercity train considered, at v_T=200 km/h, more than 85% of the displacement is caused by the frequencies excited by the wavelengths longer than the bogie-distance (λ=6.3 m). Moreover, about 10% of the displacement amplitude is caused by the wavelengths comprised between the axle-distance and the bogie-distance.

The time-domain results are compared between the first integration of accelerometers' signal with the raw data from geophones. Fig. 9 presents the signal results from both accelerometers and geophones embedded at two different depths of the track: ITL and TL. As no low-pass filters are applied to the signals, the amplitudes from accelerometers and geophones correspond to the whole frequency range (except the very low frequencies, f<1.5 Hz). The amplitude response of the particle's velocity signals seems to be identical for both sensors installed in the ITL, and a quite good result is obtained from the sensors installed in the TL with less than 0.002 m/s difference. The amplitude is higher for heavier loads: the velocity amplitude for locomotive axles is about 0.02 m/s, while the velocity amplitude measured from coach axles is about 0.01 m/s, in ITL. Comparison of the amplitudes in the ITL and TL shows that the amplitude decreases over depth. Fig. 10 presents the zooms of particle's velocity signals of the last bogie of locomotive and the first bogie of coaches for different sensors at different positions. The effect of the axle load and installation depth on the velocity signal in the time domain for both sensors can be appreciated more clearly in Fig. 10.

Table 2 Percentage of displacement amplitude measured for different cut-off frequencies for an intercity train running at 200 km/h. Each considered cut-off frequency corresponds to a different wavelength from elements of railway loading

Sensor type	Location	Load	Total reached displacement amplitude (%)			
			1/2 coach length (4.2 Hz)	Bogies (8.8 Hz)	Axles (19.8 Hz)	At 25 Hz
On sleeper	ACC Left	Locomotive	30.27	85.08	91.89	96.22
		Coach	50.73	88.36	97.16	97.57
	ACC Right	Locomotive	25.68	88.02	92.29	97.40
		Coach	52.54	88.20	95.51	97.07
Embedded	ACC-ITL (z=−0.93 m)	Locomotive	13.88	91.87	94.61	98.56
		Coach	45.89	90.75	97.95	92.29
	Geophone-ITL (z=−0.93 m)	Locomotive	22.06	95.33	96.46	99.36
		Coach	47.24	98.16	97.85	99.08
	ACC-TL (z=−1.20 m)	Locomotive	15.09	98.19	96.92	97.77
		Coach	49.51	92.23	98.30	106.80
	Geophone-TL (z=−1.20 m)	Locomotive	24.21	94.74	98.95	99.80
		Coach	60.69	91.43	96.13	98.29

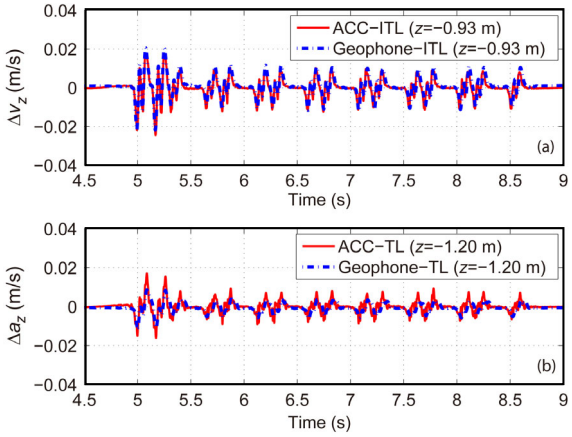

Fig. 9 Comparison between the geophone's raw signal and the first integration from accelerometers' signal at the same depth: (a) interlayer (ITL, z=−0.93 m); (b) transition layer (TL, z=−1.20 m)

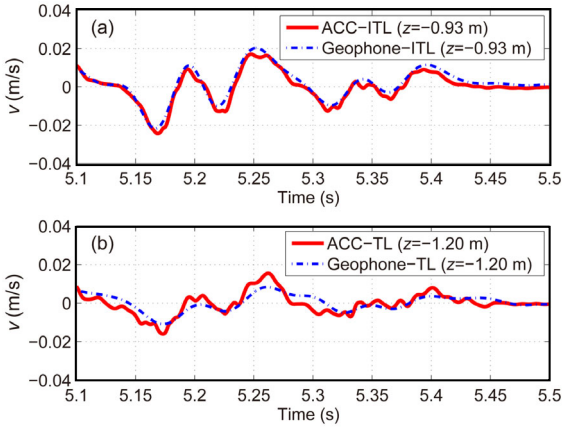

Fig. 10 Zoom on the last bogie from the locomotive and the first bogie of the coaches. Comparison between the geophone's raw signal and the first integration of the accelerometers signal at the same depth: (a) interlayer (ITL, z=−0.93 m); (b) transition layer (TL, z=−1.20 m)

The particle's velocities in ITL and TL of locomotives and coaches developed by the intercity train running at v_T=200 km/h are presented in Fig. 11. Note that the amplitude measured by the geophones is quite similar to the amplitude estimated after a first integration process of accelerometers. Differences in particle's velocity amplitudes between different kinds of axle (locomotive and coach) are significant. There is a small difference between the estimations made from different geophones and accelerometers in both instrumented depths (ITL and TL). This difference is lightly larger for the accelerometer and geophone situated in the TL. Therefore, it can be concluded that there is a good correlation between the geophone and a first integration of the accelerometer using the presented method.

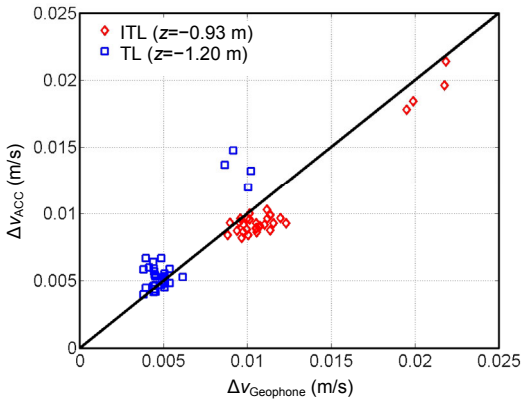

Fig. 11 Comparison between particle's velocity amplitudes estimated by a geophone and an accelerometer in two different depths (ITL and TL) caused by an intercity train running at 200 km/h

Comparison of the obtained displacements signals at three considered positions (sleeper, ITL, and TL) in Fig. 12 shows that in the ITL and TL the displacement amplitude follows the same trend for the embedded geophones and accelerometers. On sleeper (Fig. 12a), the displacement amplitudes are double (0.8 mm for locomotives and 0.5 mm for coaches) compared to the embedded amplitudes at the ITL (0.4 mm for locomotives and 0.3 mm for coaches) or quadruple compared to the TL (0.2 mm for locomotives and 0.1 mm for coaches). A zoom on results (a locomotive bogie and a coach bogie) is presented in Fig. 13. The zoom highlights the differences between LVDT deflection measurement and double-integrated accelerometer for this intercity train at 200 km/h, being more obvious the four axles' definition in the accelerometer signal. However, there is similarity between geophone and accelerometer signals for both measured depths. The differences between signals at each depth are presented in Fig. 14. This displacement difference seems larger between LVDT and accelerometer (Fig. 14a), followed by the difference between geophone and accelerometer in the TL (Fig. 14c) that is largely reduced.

To further assess the effect of train speed on the measurements, the distribution of the differences by range of speeds is analysed. This analysis is

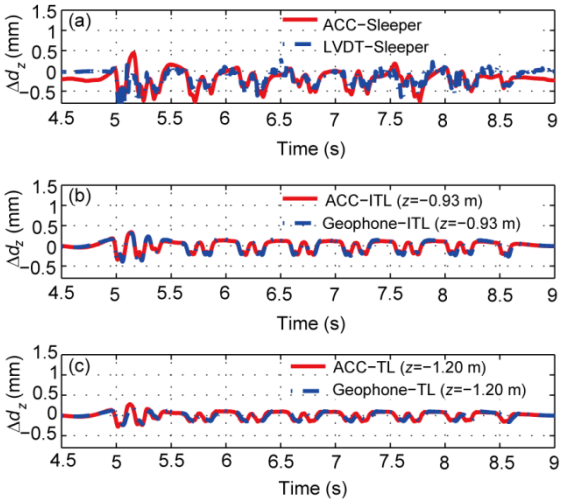

Fig. 12 Comparison between the estimated displacements of different sensors (LVDT, geophone, and accelerometer) during an intercity train passage at the three considered depths: (a) sleeper; (b) interlayer (ITL, z=−0.93 m); (c) transition layer (TL, z=−1.20 m)

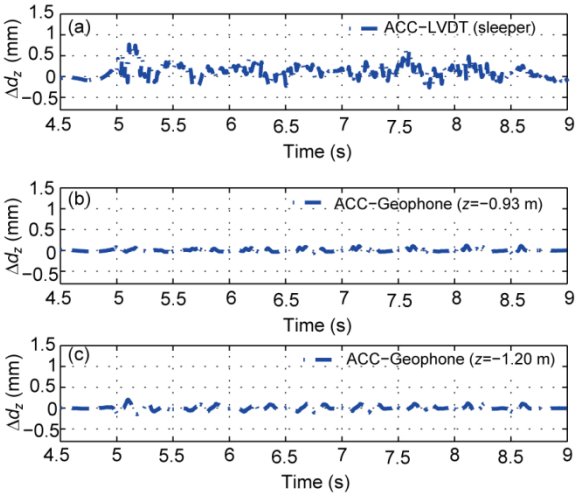

Fig. 14 Differences between estimated displacement signal of different sensors (LVDT, geophone, and accelerometer) during an intercity train passage at the three considered depths: (a) ACC–LVDT on sleeper; (b) ACC–Geophone in interlayer (ITL, z=−0.93 m); (c) ACC–Geophone in transition layer (TL, z=−1.20 m)

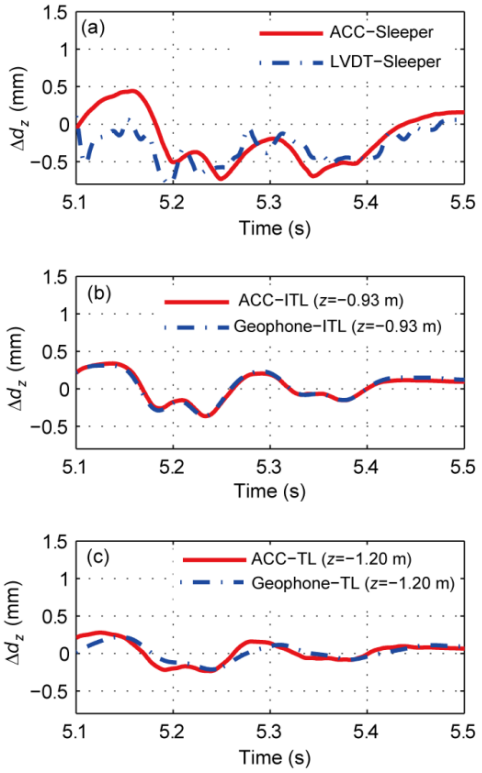

Fig. 13 Zoom on the last bogie from the locomotive and the first bogie of the coaches. Comparison between the estimated displacements from different sensors (LVDT, geophone, and accelerometer) during an intercity train passage at the three considered depths: (a) sleeper; (b) interlayer (ITL, z=−0.93 m); (c) transition layer (TL, z=−1.20 m)

performed by comparing the estimated displacement results from accelerometer with the displacement measurements of the LVDT on sleeper. Fig. 15 presents such a comparison for the 1790 train passages. It can be noted that the results are not cantered on the 1:1 line and the scatter is larger than the first integration results. However, the left side accelerometer results seem more accurate than the right side accelerometer because the LVDT measurements were performed on the left side of the sleeper. Fig. 16 presents the average scatter of the error, and it can be appreciated that the average error (compared to the LVDT measurements) is larger for the right side accelerometer, taking into account both axle loads. The average error is around 20% for both considered loads and for all range of considered train speeds. Note that the displacement amplitude error is calculated by

$$\Delta d_{\mathrm{Error}}=\frac{\left|\Delta d_{\mathrm{ACC}}-\Delta d_{\mathrm{LVDT}}\right|}{\Delta d_{\mathrm{LVDT}}}, \tag{4}$$

where $\Delta d_{\mathrm{Error}}$, Δd_{ACC}, and Δd_{LVDT} are errors in peak-to-peak displacement estimation, peak-to-peak displacement estimated with accelerometer, and peak-to-peak displacement estimated with LVDT, respectively.

To evaluate the train speed and load impact on the results of double-integration, the average and standard deviation of error between measurement and estimation from accelerometers is calculated (Table 3). It appears that heavier loads (locomotives) reduce considerably (5%) the average error when train runs faster; however, the corresponding standard deviation around the average increases by about 10%. The effect of train speed on displacement average error and the deviation, in the case of lighter loads (coaches), is much smaller compared to heavier loads. The values of average error and standard deviation for coach loadings remain stable for all the considered speeds. The same trend is found for accelerometers installed at both sides of the same sleeper with similar accelerometers. The average error of 20% obtained could be the result of some minor problems in calculating the middle-coach peak (for the peak-to-peak amplitude estimation) and the small amplitudes noise performed by high frequency excitations to the LVDT signal (which is not filtered).

In order to verify the repeatability of the measurements, a comparison of the particle's velocity results (Fig. 17) and displacement amplitude results (Fig. 18) estimated using two different accelerometers installed in the TL (z=−1.20 m) is shown. The differences between measurements of both accelerometers decrease with the increase of train speed. The average differences are around 7% for particle's velocities and 5% for displacement amplitude estimations using the presented integration method.

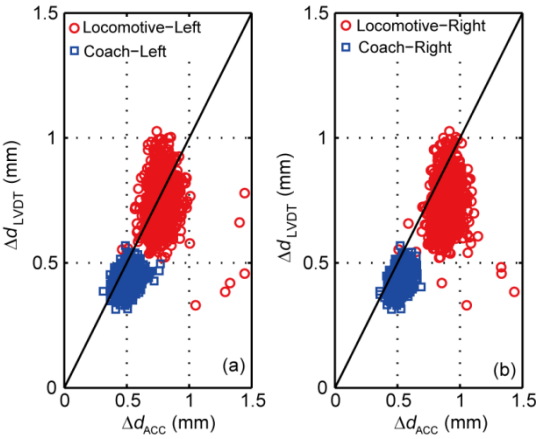

Fig. 15 Comparison between the displacement amplitudes obtained at surface from double integration of accelerometers and LVDT measurements for 1790 intercity train passages. Accelerometers installed at left (a) and right (b) sides of the sleeper. The speed of the considered trains is comprised between 80 km/h and 200 km/h

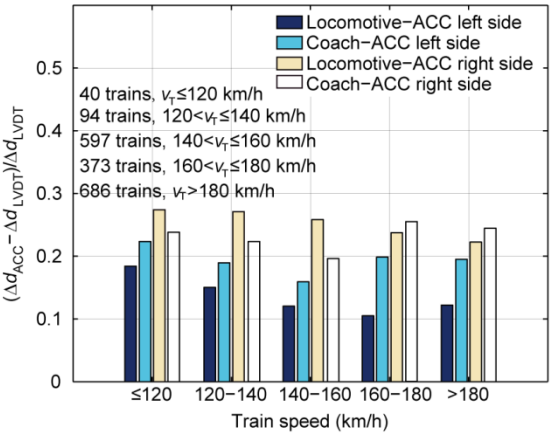

Fig. 16 Average error between displacement amplitudes obtained at surface from double integration of accelerometers signal and LVDT measurements for 1790 intercity train passages divided into five speed ranges

Table 3 Difference between displacement amplitudes, measured by an accelerometer installed at each side of a sleeper (after two integrations) and a LVDT installed on sleeper. Locomotive and coaches axles are considered

Accelerometer on sleeper		$(\Delta d_{z(ACC)}-\Delta d_{z(LVDT)})/\Delta d_{z(LVDT)}\times 100\%$*				
		v_T≤120 km/h	120 km/h<v_T ≤140 km/h	140 km/h<v_T ≤160 km/h	160 km/h<v_T≤ 180 km/h	v_T>180 km/h
ACC/Left	Locomotive	18.41±10.05	14.83±11.41	12.07±12.19	10.64±9.12	12.23±22.18
	Coach	22.35±13.16	18.53±12.69	15.78±12.18	20.81±11.93	19.55±11.49
ACC/Right	Locomotive	27.38±13.27	26.66±10.44	25.70±14.15	24.11±12.77	22.23±22.41
	Coach	23.82±9.61	22.02±11.47	19.43±11.52	26.24±10.97	24.45±10.83

* Data are presented as average±standard deviation, n=40 when v_T≤120 km/h, n=94 when 120 km/h<v_T≤140 km/h, n=597 when 140 km/h <v_T≤160 km/h, n=373 when 160 km/h<v_T≤180 km/h, and n=686 when v_T>180 km/h

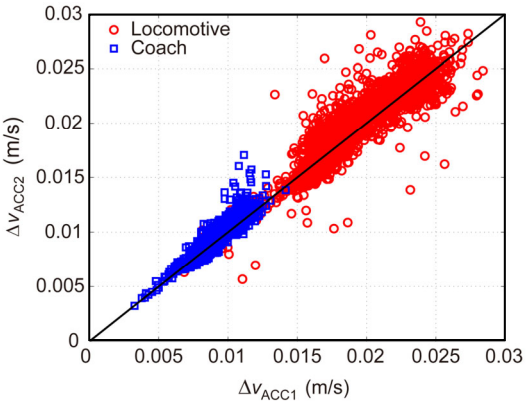

Fig. 17 Comparison between the particle's velocity amplitudes for 1790 intercity train passages, estimated from the first integration process of two accelerometers installed in the TL (z=−1.20 m)

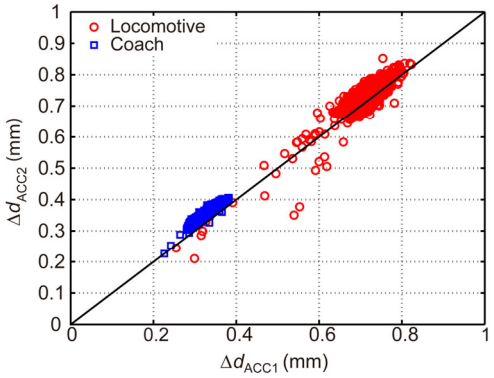

Fig. 18 Comparison between the displacement amplitudes for 1790 intercity train passages, estimated from the double-integration of two accelerometers installed in the TL (z=−1.20 m)

4 Conclusions

Based on the data from a site instrumented with accelerometers, geophones, and LVDT, the integration methods for displacement determination were assessed. The obtained results allow the following conclusions to be drawn.

The integration method is suitable for estimating the displacement amplitudes of railway track-bed materials under train loadings.

More than 95% of the displacement amplitude was caused by the excitation of the wavelengths longer than the axle-distance (λ~2.8 m), indicating that most displacement was due to the first 25 Hz frequency for a train at v_T=200 km/h.

The estimated displacements are similar for the three different sensors: accelerometers, geophones, and LVDT, validating the integration method adopted.

There is a good repeatability of the estimated displacements obtained from different sensors installed at similar locations, from the different accelerometers installed at the same sleeper for instance.

With the intercity train passages as many as 1790, the particle's velocity amplitudes per axle measured in the track-bed materials present 20% average error between the LVDT measurement and the accelerometer estimation. This average error does not depend on train speed for coach loadings; but it decreases by about 5% for heavier loads (locomotives) when train speed increases up to v_T= 200 km/h.

The repeatability of measurements was assessed using the amplitude estimation results after the first (particle's velocity) and the second integration (displacement amplitude) of two different accelerometers installed in the track-bed (TL, z=−1.20 m) for the 1790 registered intercity train passages. Note however that the validity of the integration method was proved for trains running from 80 to 200 km/h and loads from Q=105 to 225 kN/axle. For slower trains, the displacement amplitude could not be well assessed because one of the most energetic frequencies, the half-coach length, could be filtered by the applied high-pass filter and accordingly the displacement amplitudes may be underestimated. Longer monitoring is also needed to refine the analyses.

Acknowledgements

The authors are grateful to Benjamin L'HÉNORET and Jean-Michel PISSOT for their technical advice. The authors would also like to thank the track maintenance SNCF-RESEAU brigade at Vierzon, especially to their planning coordinator Ludovic GAVEAU, without whom this monitoring zone would not be accomplished.

References

Auersch, L., 1994. Wave propagation in layered soils: theoretical solution in wavenumber domain and experimental results of hammer and railway traffic excitation. *Journal of Sound and Vibration*, **173**(2):233-264. http://dx.doi.org/10.1006/jsvi.1994.1228

Boore, D.M., 2001. Effect of baseline corrections on displacements and response spectra for several recordings of the 1999 Chi-Chi, Taiwan, Earthquake.

Bulletin of the Seismological Society of America, **91**(5): 1199-1211.

Boore, D.M., 2003. Analog-to-digital conversion as a source of drifts in displacements derived from digital recordings of ground acceleration. *Bulletin of the Seismological Society of America*, **93**(5):2017-2024. http://dx.doi.org/10.1785/0120020239

Boore, D.M., Bommer, J.J., 2005. Processing of strong-motion accelerograms: needs, options and consequences. *Soil Dynamics and Earthquake Engineering*, **25**(2):93-115. http://dx.doi.org/10.1016/j.soildyn.2004.10.007

Boore, D.M., Stephens, C.D., Joyner, W.B., 2002. Comments on baseline correction of digital strong-motion data: examples from the 1999 Hector Mine, California, Earthquake. *Bulletin of the Seismological Society of America*, **92**(4):1543-1560. http://dx.doi.org/10.1785/0120000926

Bowness, D., Lock, A.C., Powrie, W., *et al*., 2007. Monitoring the dynamic displacements of railway track. *Proceedings of the Institution of Mechanical Engineers, Part F: Journal of Rail and Rapid Transit*, **221**(1):13-22. http://dx.doi.org/10.1243/0954409JRRT51

Connolly, D.P., Kouroussis, G., Fan, W.Z., *et al.*, 2013. An experimental analysis of embankment vibrations due to high speed rail. Proceedings of the 12th International Railway Engineering Conference (Railway Engineering).

Connolly, D.P., Kouroussis, G., Woodward, P.K., *et al*., 2014. Field testing and analysis of high speed rail vibrations. *Soil Dynamics and Earthquake Engineering*, **67**:102-118. http://dx.doi.org/10.1016/j.soildyn.2014.08.013

Connolly, D.P., Costa, P.A., Kouroussis, G., *et al*., 2015. Large scale international testing of railway ground vibrations across europe. *Soil Dynamics and Earthquake Engineering*, **71**:1-12. http://dx.doi.org/10.1016/j.soildyn.2015.01.001

Costa, P.A., Calcada, R., Cardoso, A.S., 2012. Track–ground vibrations induced by railway traffic: *in-situ* measurements and validation of a 2.5D FEM-BEM model. *Soil Dynamics and Earthquake Engineering*, **32**(1):111-128. http://dx.doi.org/10.1016/j.soildyn.2011.09.002

Cui, Y.J., Lamas-Lopez, F., Trinh, V.N., *et al*., 2014. Investigation of interlayer soil behaviour by field monitoring. *Transportation Geotechnics*, **1**(3):91-105. http://dx.doi.org/10.1016/j.trgeo.2014.04.002

Degrande, G., Schillemans, L., 2001. Free field vibrations during the passage of a Thalys high-speed train at variable speed. *Journal of Sound and Vibration*, **247**(1): 131-144. http://dx.doi.org/10.1006/jsvi.2001.3718

Ferreira, P.A., López-Pita, A., 2015. Numerical modelling of high speed train/track system for the reduction of vibration levels and maintenance needs of railway tracks. *Construction and Building Materials*, **79**:14-21. http://dx.doi.org/10.1016/j.conbuildmat.2014.12.124

Fröhling, R.D., 1997. Deterioration of Railway Track Due to Dynamic Vehicle Loading and Spatially Varying Track Stiffness. PhD Thesis, University of Pretoria, South Africa.

Galvín, P., Domínguez, J., 2007. Analysis of ground motion due to moving surface loads induced by high-speed trains. *Engineering Analysis with Boundary Elements*, **31**(11):931-941. http://dx.doi.org/10.1016/j.enganabound.2007.03.003

Galvín, P., Domínguez, J., 2009. Experimental and numerical analyses of vibrations induced by high-speed trains on the Córdoba–Málaga line. *Soil Dynamics and Earthquake Engineering*, **29**(4):641-657. http://dx.doi.org/10.1016/j.soildyn.2008.07.001

Graizer, V.M., 2010. Strong motion recordings and residual displacements: what are we actually recording in strong motion seismology? *Seismological Research Letters*, **81**(4):635-639. http://dx.doi.org/10.1785/gssrl.81.4.635

Hall, L., 2003. Simulations and analyses of train-induced ground vibrations in finite element models. *Soil Dynamics and Earthquake Engineering*, **23**(5):403-413. http://dx.doi.org/10.1016/S0267-7261(02)00209-9

Hendry, M.T., Barbour, L., Hughes, D.A., 2010. Track displacement and energy loss in a railway embankment. *Proceedings of the Institution of Civil Engineers-Geotechnical Engineering*, **163**(1):3-12. http://dx.doi.org/10.1680/geng.2010.163.1.3

Hendry, M.T., Martin, C.D., Barbour, S.L., 2013. Measurement of cyclic response of railway embankments and underlying soft peat foundations to heavy axle loads. *Canadian Geotechnical Journal*, **50**(5):467-480.

Kornylo, J., Jain, V., 1974. Two-pass recursive filter with zero phase shift. *IEEE Transactions on Acoustics Speech and Signal Processing*, **22**(5):384-387. http://dx.doi.org/10.1109/TASSP.1974.1162602

Kouroussis, G., Connolly, D.P., Verlinden, O., 2014. Railway-induced ground vibrations–a review of vehicle effects. *International Journal of Rail Transportation*, **2**(2):69-110. http://dx.doi.org/10.1080/23248378.2014.897791

Kouroussis, G., Caucheteur, C., Kinet, D., *et al*., 2015. Review of trackside monitoring solutions: from strain gages to optical fibre sensors. *Sensors*, **15**(8):20115-20139. http://dx.doi.org/10.3390/s150820115

Kyoya, N., Arakawa, K., 2009. A method for impact noise reduction from speech using a stationary-nonstationary separating filter. International Symposium on Communications and Information, p.33-37.

Lamas-Lopez, F., Cui, Y.J., Calon, N., *et al.*, 2016a. Geotechnical auscultation of a French conventional railway track-bed for maintenance purposes. *Soils and Foundations*, **56**(2):240-250. http://dx.doi.org/10.1016/j.sandf.2016.02.007

Lamas-Lopez, F., Cui, Y.J., Calon, N., *et al*., 2016b. Track-bed mechanical behaviour under the impact of train at different speeds. *Soils and Foundations*, **56**(4):627-639. http://dx.doi.org/10.1016/j.sandf.2016.07.004

Le Pen, L., Watson, G., Powrie, W., *et al*., 2014. The behaviour of railway level crossings: insights through field monitoring. *Transportation Geotechnics*, **1**(4):201-213. http://dx.doi.org/10.1016/j.trgeo.2014.05.002

Madshus, C., Kaynia, A.M., 2000. High-speed railway lines on soft ground: dynamic behaviour at critical train speed. *Journal of Sound and Vibration*, **231**(3):689-701. http://dx.doi.org/10.1006/jsvi.1999.2647

Mishra, D., Tutumluer, E., Boler, H., *et al*., 2014. Instrumentation and performance monitoring of railroad track transitions using multidepth deflectometers and strain gauges. 93rd Annual Meeting of the Transportation Research Board.

Müller-Boruttau, F.H., Breitsamer, N., 2004. Elastic Elements Reduce the Loads Exerted on the Permanent Way. Technical Note, Beratende Ingenieure BYIK, Germany.

Priest, J.A., Powrie, W., 2009. Determination of dynamic track modulus from measurement of track velocity during train passage. *Journal of Geotechnical and Geoenvironmental Engineering*, **135**(11):1732-1740. http://dx.doi.org/10.1061/(ASCE)GT.1943-5606.0000130

Priest, J.A., Powrie, W., Grabe, P.J., *et al*., 2010. Measurements of transient ground movements below a ballasted railway line. *Géotechnique*, **60**(9):667-677. http://dx.doi.org/10.1680/geot.7.00172

Stiros, S.C., 2008. Errors in velocities and displacements deduced from accelero-graphs: an approach based on the theory of error propagation. *Soil Dynamics and Earthquake Engineering*, **28**(5):415-420. http://dx.doi.org/10.1016/j.soildyn.2007.07.004

Thong, Y.K., Woolfson, M.S., Crowe, J.A., *et al*., 2002. Dependence of inertial measurements of distance on accelerometer noise. *Measurement Science and Technology*, **13**(8):1163-1172. http://dx.doi.org/10.1088/0957-0233/13/8/301

Trifunac, M.D., 1971. Zero baseline correction of strong-motion accelerograms. *Bulletin of the Seismological Society of America*, **61**(5):1201-1211.

Yang, J., Li, J.B., Lin, G., 2006. A simple approach to integration of acceleration data for dynamic soil–structure interaction analysis. *Soil Dynamics and Earthquake Engineering*, **26**(8):725-734. http://dx.doi.org/10.1016/j.soildyn.2005.12.011

Zuada-Coelho, B.E., 2011. Dynamics of Railway Transition Zones in Soft Soils. MS Thesis, University of Porto, Portugal.

中文概要

题　目：利用现场测试的加速度和速度数据确定位移的积分方法评价

目　的：本文旨在研究不同波长载荷（包括车厢长度、构架长度以及轴距等）对位移确定的影响，利用积分方法确定位移的有效性和重复性的适用范围，以及研究列车速度和轴荷载对变形量的影响，为轨道基础位移监测提供重要的方法。

创新点：1. 评价和分析一种积分方法，该方法利用低通滤波法但不消除产生变形的主要频率；2. 通过对位移、速度和加速度传感器在时域和频域结果的比较，使重复性得到保证。

方　法：利用线性可变差位移传感器、地震检波器以及加速度计获取轨道不同深度的位移、速度和加速度，然后利用巴特沃兹低通滤波器对 3 类数据进行滤波。通过对速度一阶积分、加速度二阶积分，获得由 3 种传感器测试得到的位移并验证其准确性。

结　论：通过测试和分析发现，95%的位移幅值来自于波长大于轴距（2.8 m）的激励，对应的低频为 25 Hz（列车运行速度为 200 km/h）。通过线性可变差位移传感器、地震检波器以及加速度计直接获得或间接积分获得的位移十分接近，验证了积分方法的有效性，且其具有较高的可重复性。

关键词：铁路轨道；振动；加速度计；地震检波器；线性可变差位移传感器；积分方法；变形量估计；测试重复性